



HAL
open science

Mercury, organic matter, iron, and sulfur co-cycling in a ferruginous meromictic lake

Delphine Tisserand, Stéphane Guédron, Eric Viollier, Didier Jézéquel, Sylvain Rigaud, Sylvain Campillo, Geraldine Sarret, Laurent Charlet, Daniel Cossa

► To cite this version:

Delphine Tisserand, Stéphane Guédron, Eric Viollier, Didier Jézéquel, Sylvain Rigaud, et al.. Mercury, organic matter, iron, and sulfur co-cycling in a ferruginous meromictic lake. *Applied Geochemistry*, 2022, 146, pp.105463. 10.1016/j.apgeochem.2022.105463 . hal-03801098

HAL Id: hal-03801098

<https://hal.inrae.fr/hal-03801098>

Submitted on 15 Nov 2022

HAL is a multi-disciplinary open access archive for the deposit and dissemination of scientific research documents, whether they are published or not. The documents may come from teaching and research institutions in France or abroad, or from public or private research centers.

L'archive ouverte pluridisciplinaire **HAL**, est destinée au dépôt et à la diffusion de documents scientifiques de niveau recherche, publiés ou non, émanant des établissements d'enseignement et de recherche français ou étrangers, des laboratoires publics ou privés.



Distributed under a Creative Commons Attribution - NonCommercial - NoDerivatives 4.0 International License

Mercury, organic matter, iron, and sulfur co-cycling in a ferruginous meromictic lake

APPLIED GEOCHEMISTRY 146 (2022) 105463

<https://doi.org/10.1016/j.apgeochem.2022.105463>

Delphine Tisserand^a, Stéphane Guédron^{a*}, Eric Viollier^b, Didier Jézéquel^{b,c}, Sylvain Rigaud^d,
Sylvain Campillo^a, Géraldine Sarret^a, Laurent Charlet^a, and Daniel Cossa^a

^a *ISTerre, Univ. Grenoble Alpes, Univ. Savoie Mont Blanc, CNRS, IRD, Univ. Gustave Eiffel, F-38000 Grenoble, France*

^b *Université Paris Cité, Institut de Physique du Globe de Paris, 1 rue Jussieu, F-75238 Paris Cedex 05, France*

^c *CARTELE, INRAE et Univ. Savoie Mont Blanc, 75 bis Avenue de Corzent, F-74200 Thonon-les-Bains, France*

^d *Univ. Nîmes, EA 7352 CHROME, Rue Du Dr Georges Salan, F-30021 Nîmes, France*

**Corresponding author: stephane.guedron@ird.fr*

Abstract

Mercury (Hg) speciation in natural waters is controlled by redox conditions and microbiological activity. Water columns of meromictic lakes have large and stable redox chemical and biological gradients that allow the investigation of many Hg chemical transformations. In this study, Hg speciation (elemental Hg = Hg⁰, methylated Hg = MeHg) and partitioning between truly dissolved (< 3 kDa), colloidal (< 0.45 μm and > 3 kDa), and particulate (> 0.45 μm) fractions, were determined throughout a high-resolution water column profile in the ferruginous meromictic Lake Pavin (Massif Central, France) in July 2018. Total Hg concentrations (THg) in water ranged between 0.4 to 8.8 pmol L⁻¹. The particulate phase represented 10 to 70% of the THg, with a peak found in the mesolimnion associated with the particulate organic carbon maximum. In the mesolimnion, the colloidal fraction represented 12 to 68% of THg, and the highest value was found at the top of the sulfidic zone, whereas the truly dissolved Hg species (70 ± 9%) dominated in all the rest of the sulfidic zone. MeHg ranged from less than 10% of THg in the oxic mixolimnion to more than 90% in the anoxic monimolimnion. The Hg methylation was most active within the suboxic zone where iron and sulfate reduction are occurring. These results, associated with those of the partition of organic matter (OM), sulfur, and iron, in conjunction with thermodynamic calculations, allow us to present a conceptual scheme for the Hg cycle in the lake. Atmospheric Hg deposited onto surface waters of the lake is partially photo-reduced and returned to the air, another part is scavenged by biogenic particulate matter and conveyed at depth by settling organic material. Water stratification and redox changes create a sequence of reactions from oxic to ferruginous waters where Hg is successively (i) desorbed from particulate OM where mineralization occurs, (ii) adsorbed onto iron-oxy(hydr)oxides, (iii) desorbed where they dissolved, (iv) precipitate as HgS, (v) methylated, and (vi) reduced as Hg⁰ in the deepest part of the lake. In brief, the (micro)biological uptake, OM, iron and sulfur recycling, through associated microbial consortia, control the Hg cycling in the Pavin waters.

Keywords: Mercury; methylmercury; redox; iron; sulfur; organic matter; Lake Pavin

1 **1. INTRODUCTION**

2 Mercury (Hg) is present in natural waters mainly in two oxidation states (0 and II). The
3 zerovalent form is the dissolved gaseous elemental Hg (Hg^0), and the divalent forms (Hg^{II}) are
4 often tightly bound to sulfur (S) and carbon (C) (Wang et al., 2022; Xia et al., 1999). Hg^{II} forms
5 preferentially strong complexes with reduced inorganic sulfur and organic matter (OM) via
6 sulfhydryl (-SH) groups (Dyrssen and Wedborg, 1991; Riccardi et al., 2013). It also forms
7 covalent bonds with C (Barone et al., 1996), which leads to the natural occurrence of the highly
8 toxic methylated Hg (MeHg) compounds, including its two forms; i.e., monomethylmercury
9 (MMHg), and the volatile dimethylmercury (DMHg). On the other hand, Hg-S affinity explains
10 the dominant association of Hg with natural OM enriched in reduced S functional groups (Loux,
11 1998). The biogeochemical cycle of Hg in natural waters involves numerous thermal, photo,
12 and biogenic reactions. Among them, two reversible and competitive Hg transformations are
13 crucial from an aquatic ecology point of view: oxidation-reduction and methylation-
14 demethylation. Indeed, reduction of Hg^{II} leads to the formation of volatile Hg^0 that can escape
15 from the aquatic environment, and methylation leads to the formation of MMHg that, through
16 its biomagnification in aquatic food webs, is harmful to fish consumers. For this latter reaction,
17 microbial activity is crucial and largely dominates abiotic production (Cooper et al., 2020; Parks
18 et al., 2013; Regnell and Watras, 2018; Ullrich et al., 2001). These reactions occur particularly
19 in hypoxic and anoxic environments (Fitzgerald et al., 2014; Mason et al., 2012), making the
20 Hg cycling in natural waters strongly dependent on redox conditions (Mason et al., 1999). In
21 addition to reactions occurring in the dissolved phase, Hg may precipitate as sulfur minerals
22 (*e.g.*, cinnabar) in euxinic environment, and is involved in heterogeneous reactions, such as
23 sorption onto various minerals, including iron minerals like goethite (Kim et al., 2004; Slowey
24 and Brown, 2007) and mackinawite (Jeong et al., 2007). Numerous studies have documented
25 the main Hg changes in speciation and partitioning where strong redox gradients are present,
26 such as in surficial sediments of lakes and coastal zones (Feyte et al., 2010; Gobeil and Cossa,
27 1993; Merritt and Amirbahman, 2007). However, the complexity and diversity of Hg
28 transformations are difficult to distinguish in sedimentary deposits where redox changes occur
29 at millimeter or centimeter-scale. On the contrary, they are easily characterized at high
30 resolution in water columns where redox gradients may extend over several meters. Indeed, Hg
31 enrichment and major changes in speciation have been identified at the interfaces between oxic
32 and anoxic waters (Cossa and Coquery, 2005; Guédron et al., 2020b; Iverfeldt, 1988; Lamborg
33 et al., 2008; Mercone et al., 1999; Muresan et al., 2008). The high-resolution (1 cm) study of a

34 stratified water column in a tropical dam lake, showed prominent Hg methylation intricately
35 linked with Hg⁰ production at the chemocline (Muresan et al., 2018). Both reactions were found
36 to be fueled by nutrients released episodically during the decomposition of settling OM or
37 inhibited by dissolved OM and inorganic compounds continuously transported from the deeper
38 layer. Hence, the chemocline acts as both an accumulation and recycling domain for settling
39 MeHg-loaded organic particles.

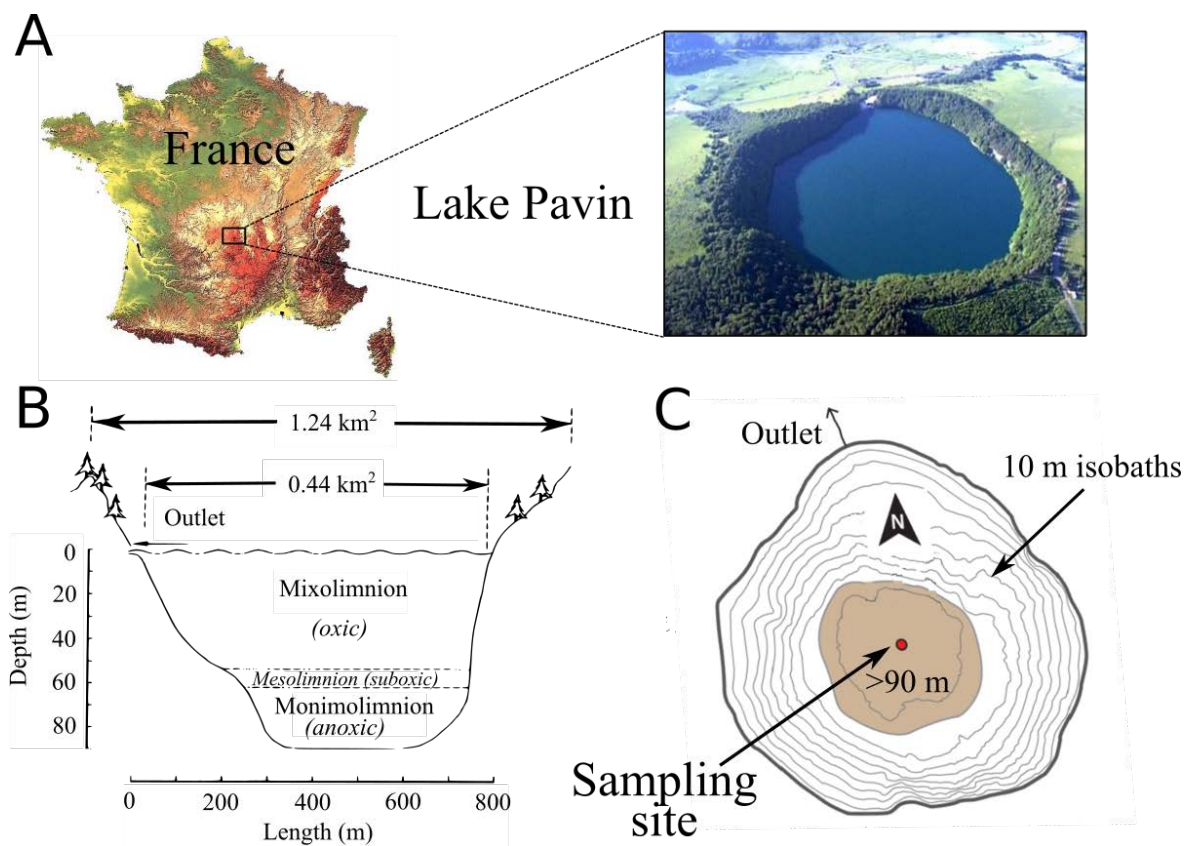
40 The water column of meromictic lakes is permanently stratified. Lake Pavin (France) is a good
41 example of such a situation; it offers a unique natural geochemically well-described laboratory
42 (Bura-Nakic et al., 2009; Busigny et al., 2016; Jézéquel et al., 2016; Viollier et al., 1997), where
43 Hg transformations can be studied in detail. Only one study has previously described the
44 distribution of the Hg species in Lake Pavin (Cossa et al., 1994). With the analytical tools
45 available at that time, the authors described the MeHg formation at the redoxcline and suggested
46 an influence of Fe and Mn recycling on Hg partitioning and speciation. More recently, HgS
47 nanoparticles have been identified in the monimolimnion (Miot et al., 2016). The present study
48 is the first to focus on Hg distribution, speciation, and partitioning in the oxic-anoxic transition
49 zone of a meromictic lake using 1 m vertical resolution profiles and which documents their
50 relation to Fe, S, and OM redox cycling. In addition, the use of thermodynamic calculations
51 codes on this dataset allowed us to better understand dissolved speciation and solution
52 equilibrium state with respect to mineral phases in order to construct a comprehensive
53 biogeochemical model for Hg cycling in the lake.

54 **2. MATERIAL AND METHODS**

55 **2.1. Study site**

56 Lake Pavin (45°55'N, 2°54'E, Fig. 1) is a trachytic maar, located in the Massif Central (France),
57 at an altitude of 1197 m. The lake was formed ~ 6900 years ago (Chapron et al., 2010; Juvigné
58 et al., 1996) during a strong phreatomagmatic explosion (Thouret et al., 2016). The lake is a
59 nearly circular depression of *ca.* 750 m in diameter and 92 m depth, with an area of 0.445 km²
60 and a truncated cone topography. Its watershed is estimated to be 1.24 km² (Michard et al.,
61 1994). The average discharge of Lake Pavin is 50 L.s⁻¹ (Thouret et al., 2016). Because of its
62 geometry, wind protection, and sub-lacustrine springs, the mixing of the Pavin water column is
63 depth-limited (Bonhomme et al., 2016; Busigny et al., 2016). Lake Pavin is a ferruginous
64 meromictic lake, composed of two main layers: (i) the mixolimnion, which extends from the
65 surface to 50-60 m depth and is oxygenated due to the seasonal mixing, and (ii) the permanently
66 anoxic monimolimnion, which extends down to the lake bottom (92 m) and contains very high

67 concentrations of dissolved elements which contribute to the stability of the layer (Martin, 1985;
 68 Michard et al., 1994; Viollier et al., 1997). The residence time of the waters is estimated
 69 between about 9 years in the mixolimnion and 100 years in the monimolimnion (Jézéquel et al.,
 70 2016). In between, is a transition zone, called the mesolimnion (sometimes considered as the
 71 upper part of the monimolimnion), which is characterized by a strong decrease in oxygen and
 72 redox potential, and a strong increase in specific conductivity (Lopes et al., 2011; Busigny et
 73 al., 2021). It is worth noting that the vertical positions of the oxycline, the redoxcline and the
 74 chemocline in the water column may change by a few meters depending on seasons
 75 (Bonhomme et al., 2011).



76

77 **Figure 1.** Lake Pavin: A) location in the Massif Central (France) and aerial photography (Credit: D.
 78 Jézequel, CNRS Images), B) morphological characteristics of the lake, and C) bathymetric map and
 79 sampling site location adapted from Chassiot et al (2016).

80

81 2.2. Sample collection and storage

82 Sampling was performed in July 2018 from the middle of the lake (Fig. 1) on a floating platform
 83 using a PFA pneumatic pump (AstiPure™, Saint-Gobain) with a 100-meter-long polyethylene
 84 (0.9 cm diameter) tubing. Samples were collected without any contact with the atmosphere at
 85 1 m depth-intervals in the mesolimnion (52-65 m), and 10 m depth intervals elsewhere. Redox
 86 potential (Eh), conductivity, and pH were measured *in situ* with probes connected to a WTW

87 multi 340i. Filtrations for Hg speciation, anions, major, trace, and redox-sensitive elements
88 were performed on site onto hydrophilic 0.45 μm PTFE filters (OmniporeTM). Filters were then
89 used for the analysis of total particulate Hg (THg_P), and particulate major and trace elements.
90 Filtered and unfiltered samples for total Hg (THg_F and THg_{UNF}) and methylmercury (MeHg_F
91 and MeHg_{UNF}) analyses were collected and stored into acid-cleaned FEP Teflon bottles
92 following ultra-clean techniques (Cossa and Gobeil, 2000). In the mesolimnion, additional
93 samples were ultra-filtrated on site on pre-cleaned membranes (<3 kDa, Vivaspin®,
94 polyethersulfone (PES), by centrifugation (6900 rpm, 4°C during 60 min), for the determination
95 of the “truly-dissolved” THg (THg_{UF}) (Guédron et al., 2016). The colloidal part of the THg_F,
96 i.e., THg_{coll}, was then obtained from the difference between THg_F and THg_{UF}. All samples for
97 Hg analysis were acidified (0.4 % v/v) on-site with HCl (Optima[®] grade), except those for
98 dissolved gaseous mercury (DGM = Hg⁰ + DMHg) determinations, which were kept unfiltered
99 in the dark at +4°C until the analysis. Samples for major and trace elements were stored in
100 polyethylene vials and acidified with HNO₃ (1 % v/v, Suprapur[®] grade). Samples for dissolved
101 organic carbon (DOC) analyses were filtered through glass fiber filters (<0.7 μm , GFF). Filters
102 were then cut in equal parts used for the analysis of particulate organic carbon (POC), THg_P
103 and particulate methylmercury (MeHg_P). DOC samples were stored in borosilicate vials and
104 acidified with HCl (0.2 % v/v). All samples were wrapped in double bags and kept in the dark
105 at +4 °C until analysis.

106 **2.3. Mercury speciation and partitioning**

107 Filtered, unfiltered, and ultra-filtered THg, and DGM in water were measured by CV-AFS
108 (Tekran[®], model 2500) following the published US-EPA Standard Method N° 1631 (Bloom,
109 1996; Cossa et al., 2003; USEPA, 2002). The detection limit was 0.5 pmol L⁻¹ for a 40-mL
110 water aliquot and the reproducibility varied between 5 and 15 % (N = 6) according to the
111 concentration level in the samples. The accuracy of THg measurements was tested using the
112 certified reference material (CRM) ORMS-5 (certified value = 26.2 \pm 1.3 pg g⁻¹) from the
113 National Research Council of Canada. DGM was quantified by purging 500 mL of unfiltered
114 water with Hg-free argon within two hours after sample collection (Cossa et al., 2017). Filtered
115 and unfiltered MeHg (= MMHg + DMHg) were quantified following the derivatization method
116 based on an aqueous ethylation, and purge-trap on a Tenax[®], gas chromatography, and cold
117 vapor atomic fluorescence spectrometry (CV-GC-AFS) with a Tekran[®] detector (model 2700)
118 following the US-EPA 1630 protocol (USEPA, 1998). The precision of analysis was
119 determined by measuring replicates of a control standard (RSD < 10 %, N=20), and the absence

120 of matrix effect was verified using the standard addition technique (Guédron et al., 2011;
121 Guédron et al., 2017). Total particulate Hg and MeHg (THg_P, MeHg_P) concentrations were
122 determined with the same method as for solution, after the digestion of Hydrophilic PTFE
123 membranes with HNO₃:HCl mixture (2:1 v:v, 70 °C, 48 h) for THg_P, and after the digestion of
124 GF/F membranes with HNO₃ (6 N, 70 °C, 24 h) for MeHg_P. The QA/QC was checked with two
125 CRMs, MESS-3 and IAEA-405, for THg and MeHg respectively. Recovery was 100 ± 10% for
126 the two methods, and precision was better than 15% for THg_P (n = 6) and better than 5% for
127 MeHg_P (n = 5).

128 **2.4. Major, trace elements, and organic matter analyses**

129 Particulate major and trace elements were quantified on an aliquot of the digestion solution
130 used for the THg_P determination (PTFE filters). Total Fe and Mn concentrations and trace
131 elements (Cu, Cd, Co, Ni, Zn, Pb, Cr) were quantified with an ICP-MS (Thermo[®], X-series 2).
132 Precision was assessed by replicate analysis of CRM SLRS-4, with values better than 7% for
133 all studied elements. Major (Ca, K, Mg, Na, P, S, Si, Sr) were quantified by inductively coupled
134 plasma atomic emission spectrometry (ICP-AES, Varian 720 ES model). The precision was
135 better than ± 5%. Ferrous iron (Fe^{II}) was determined on-site using the ferrozine method (Viollier
136 et al., 2000) with a portable spectrophotometer. Sulfides ($\Sigma\text{H}_2\text{S} = \text{H}_2\text{S} + \text{HS}^- + \text{S}^{2-}$) samples
137 were measured on-site with a portable spectrophotometer following Cline's method (Cline,
138 1969) on filtered water stabilized directly after filtration with 0.01 M zinc acetate (Tisserand et
139 al., 2021). Calibration was performed using an external standardization from a solution
140 prepared with Na₂S.9H₂O and titrated by an iodometric method (USGS, 2002). Anions [(i.e.,
141 chloride (Cl⁻), sulfates (SO₄²⁻), nitrates (NO₃⁻), and total dissolved phosphates (TDP)] were
142 measured by ion chromatography (IC 332, Metrohm[®]), with a precision better than 1 %. DOC
143 was measured with a TOC-VCSN analyzer (Shimadzu[®]). POC and was quantified with a mass
144 spectrometer (SERCON[®]) after combustion of GF/F filters at 1000 °C (Raimbault et al., 1999).
145 The detection limit and precision were estimated at 10 µg and 5%, respectively. Finally,
146 suspended particulate matter (SPM) was reconstructed from the organic and inorganic content
147 of particles collected on filters (Prahl et al., 1997).

148 **2.5. Thermodynamic calculations**

149 WHAM 7 (Tipping, 1994) and PHREEQC 3.0 (Parkhurst and Appelo, 2013) softwares were
150 combined following the method of crossed modeling described in Rigaud *et al.* (2013) for the
151 determination of (i) aqueous Hg^{II} and MeHg speciations, and (ii) mineral phase equilibrium
152 accounting for redox gradient and dissolved OM complexation. The THERMODDEM default

153 database (<https://thermoddem.brgm.fr/>) was used and implemented with all reactions involving
 154 dissolved Hg and MeHg known in the literature [Tab. SI.1 and 2 (Blanc et al., 2018; Drott et
 155 al., 2013; Feyte et al., 2012; Skyllberg, 2008; Smith and Martell, 1976)]. Calculations were
 156 firstly performed with WHAM and the calculated apparent thermodynamic constants (K_{app}) of
 157 the complexation reactions between aqueous Hg^{II} and MeHg and humic acid (HA) and fulvic
 158 acids (FA) were then added to the database for PHREEQC calculations. Temperature, pH,
 159 dissolved molar concentrations in dissolved inorganic Hg (THg-MeHg) and MeHg, HA, FA,
 160 Hg, Fe, Mn, ΣH_2S , major cations and anions were defined as input parameters in both models
 161 (Tabs. SI.3 and 4). HA and FA molar concentrations were calculated from Eq. 1 and 2:

$$162 \quad HA_{mol\ L^{-1}} = 2 \times 0.1 \times DOC_{mg\ L^{-1}} \times 10^{-3} / M_{HA-g\ mol^{-1}} \quad (Eq. 1)$$

$$163 \quad FA_{mol\ L^{-1}} = 2 \times 0.9 \times DOC_{mg\ L^{-1}} \times 10^{-3} / M_{FA-g\ mol^{-1}} \quad (Eq. 2)$$

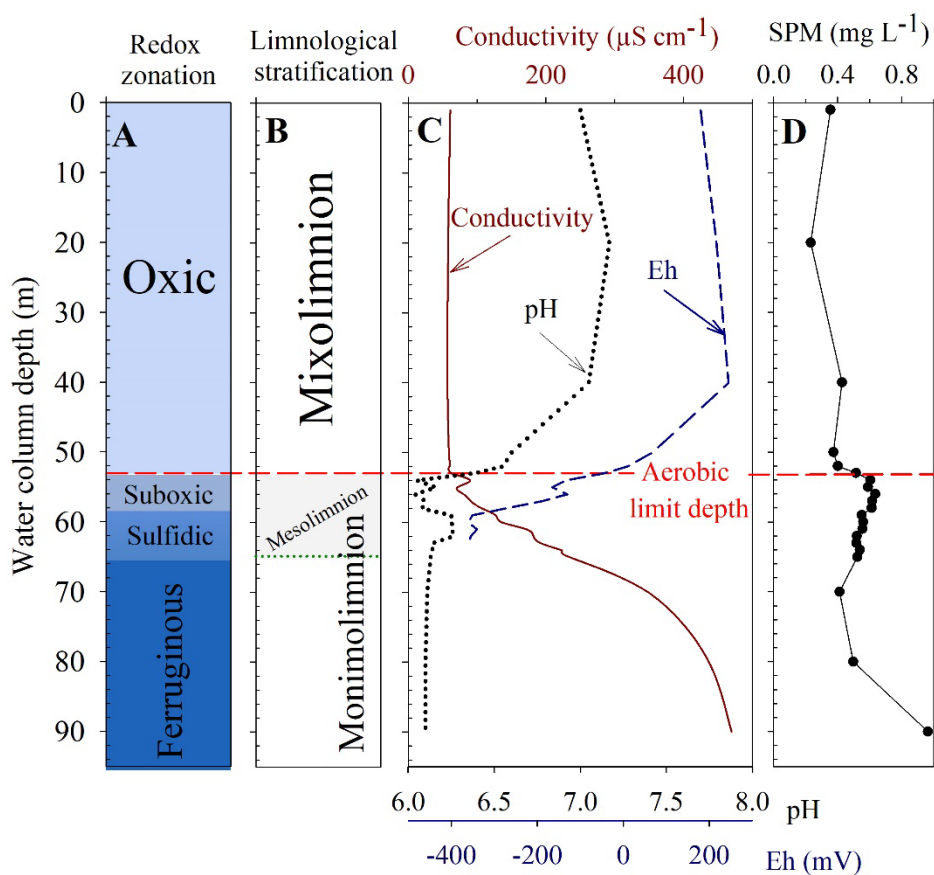
164 considering a dissolved organic matter to DOC ratio of 2:1, and a FA:HA mass ratio of 9:1 with
 165 $M_{HA} = 650\ g.mol^{-1}$ and $M_{FA} = 2000\ g.mol^{-1}$ (Buffle and Chalmers, 1988; Malcolm, 1985).
 166 Saturation indices (SI) were calculated for 47 mineral phases containing Hg, Fe, S, and Mn,
 167 including 11 Hg mineral phases (Tab. SI.2).

168 3. RESULTS

169 3.1. Water column chemistry

170 Figure 2 illustrates the successions of the redox (Fig. 2A) and physical (Fig. 2B) structures of
 171 the water column of Lake Pavin during the sampling period. The mixolimnion was spread
 172 between 0 and 53 m depth and the monimolimnion from 53 m down to 92 m including the
 173 mesolimnion between 54 m and 65 m. The aerobic limit was observed at 53 m (Fig. 2). The
 174 water conductivity was stable in the mixolimnion with an average value of $60\ \mu S\ cm^{-1}$, and
 175 increased in the mesolimnion to reach $470\ \mu S\ cm^{-1}$ in the monimolimnion (Fig. 2C). Major
 176 elements concentration profiles in the filtered fraction depicted similar patterns parallel to the
 177 conductivity (Fig. SI.1). The pH decreased from 7.0 at the surface to 6.1 at the bottom of the
 178 lake, with a marked gradient in the suboxic layer (Fig. 2C). Redox values (Eh) were high in the
 179 mixolimnion, and started to decline with increasing depth from 40 m down to 58 m, *i.e.*, the
 180 bottom of the suboxic zone (Fig. 2C). Suspended particulate matter (SPM) was quite
 181 homogenous and low in the mixolimnion, and increased markedly around the oxycline as well
 182 as at the bottom of the lake in the nepheloid layer (Busigny et al., 2014) up to $0.96\ mg\ L^{-1}$ (Fig.
 183 2D). DOC concentrations (Fig. 3A) averaged $90.4 \pm 13.6\ \mu mol\ L^{-1}$, and increased gradually

184 from the top of the monimolimnion up to $354 \mu\text{mol L}^{-1}$ at the bottom of the lake. POC
 185 concentrations increased in the mesolimnion from an average concentration of $11.5 \pm 5 \mu\text{mol}$
 186 L^{-1} in the mixolimnion to $21.4 \pm 2 \mu\text{mol L}^{-1}$ in the monimolimnion. The high value at 90 m (\sim
 187 $39 \mu\text{mol L}^{-1}$) suggests that particles from the nepheloid layer were sampled. Total dissolved
 188 phosphates (TDP) were only measurable below 65 m depth and increased rapidly in the
 189 monimolimnion up to 0.5 mmol L^{-1} at 70 m depth. Particulate phosphorus (P_P) increased
 190 steadily from negligible values above 54 m (*i.e.*, above the oxycline), up to 0.3 mmol L^{-1} at the
 191 lake bottom (Fig. 3B).

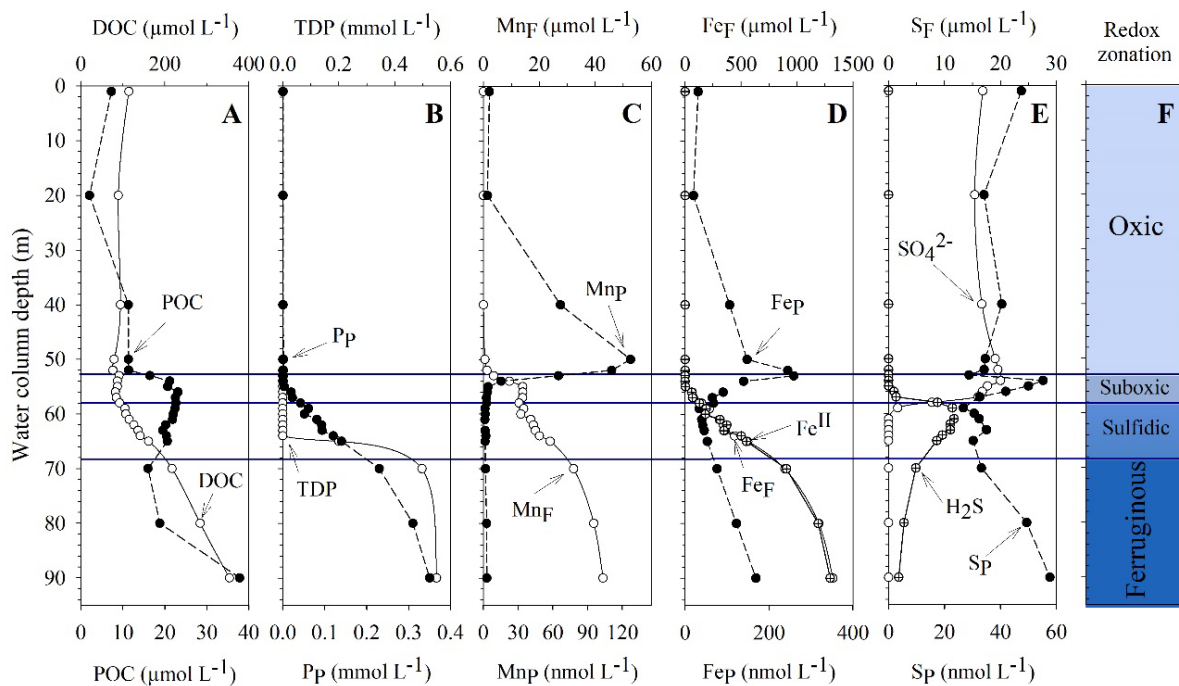


192

193 **Figure 2.** Vertical zonation of Lake Pavin water column based on (A) redox domains, (B) water
 194 limnological stratification, (C) electrical conductivity, pH, redox potential (Eh), and (D) suspended
 195 particulate matter (SPM) concentrations measured in July 2018.

196 Consistent with the definitions by Froelich et al. (1979), Poultron and Canfield (2011), and
 197 Busigny et al. (2016), four redox zones were identified in the water column of Lake Pavin (Fig.
 198 2A): (i) the oxic zone where molecular oxygen is still present (0-53 m); (ii) the suboxic zone
 199 without molecular oxygen, but where other electron acceptors, such as Fe^{III} , Mn^{IV} , or S^{VI} , are
 200 present (54-59 m); (iii) the sulfidic zone where the $\Sigma\text{H}_2\text{S}$ is abundant (60-65 m); and (iv) the
 201 ferruginous layer where Fe^{II} prevails (65-90 m). Zone (i) belongs to the mixolimnion, zones (ii)

202 and (iii) to the mesolimnion, and zone (iv) to the monimolimnion. Peaks of Fe_P and Mn_P are
 203 encountered above and at the interface between the oxic and suboxic layer, respectively,
 204 presumably because of precipitation of Fe and Mn diffusing upwards. There, neoformed
 205 oxy(hydr)oxides may have adsorbed dissolved organic matter and contribute to the POC peak.
 206 In the suboxic zone, Mn_P and Fe_P (Fig. 3C and D) started to decrease successively from 52 and
 207 54 m depth, respectively. Consistently, dissolved Mn and Fe concentrations showed a mirrored
 208 increase in the form of reduced species as all dissolved Fe is found in its reduced form (Fe^{II}).
 209 The reduction of SO_4^{2-} started below 54 m, ΣH_2S appeared at 58 m and peaked up to $11 \mu\text{mol}$
 210 L^{-1} around 62 m (Fig. 3E). It is worth mentioning that the sulfidic zone (zone with ΣH_2S) was
 211 identified between 58 and 65 m, i.e., overlapping the onset of the ferruginous zone.
 212 These phase changes are also consistent with the conventional succession of redox
 213 biogeochemical reactions along the redox gradient, which trigger reductive dissolution of the
 214 oxy(hydr)oxides (Froelich et al., 1979), as already noticed in Lake Pavin by Viollier et al.
 215 (1997). Because of the limited amount of sulfur in the lake, ferruginous conditions set in the
 216 monimolimnion confers the singular characteristic to Lake Pavin (Bura-Nakic et al., 2009).



217

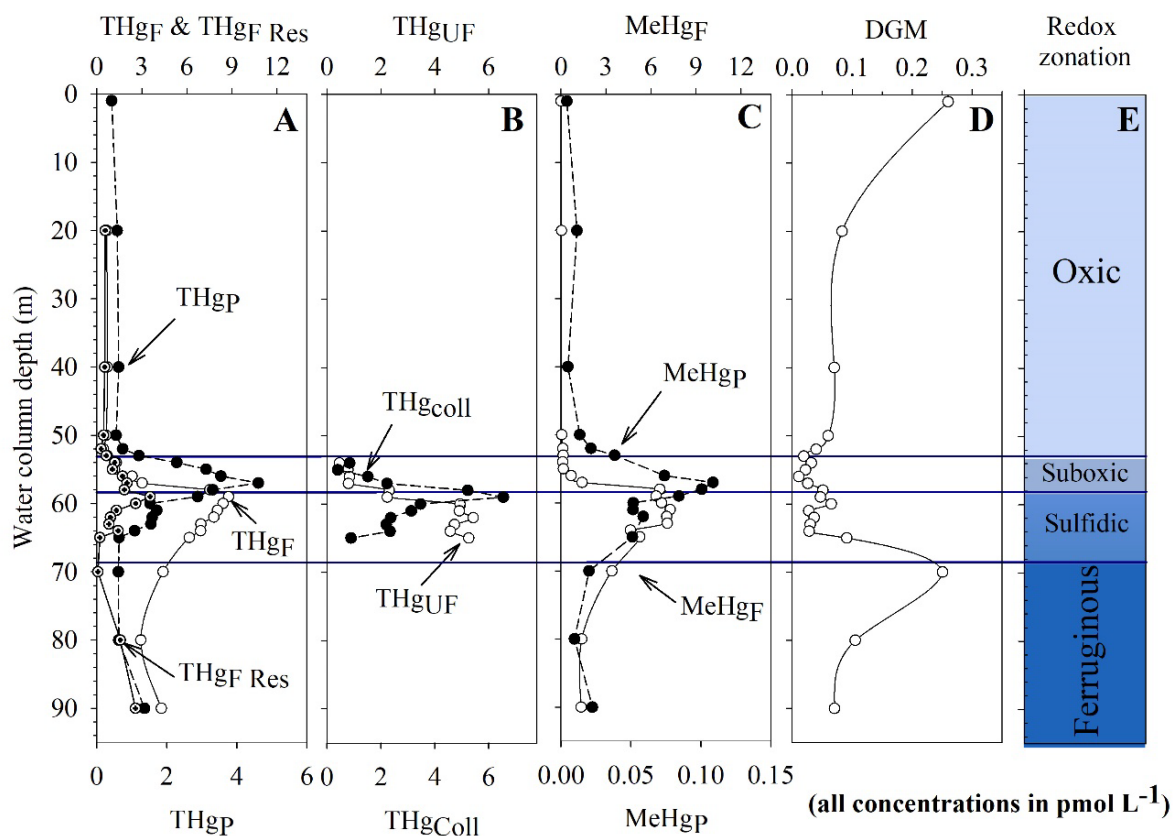
218 **Figure 3.** Depth concentration profiles of dissolved and particulate (A) organic carbon, (B) phosphorus,
 219 (C) manganese, (D) iron, and (E) sulfur (sulfate, and sulfides) in the water column of Lake Pavin.
 220 Subscript F refers to filtered samples and subscript P to the particulate phase. The light blue band
 221 indicates the oxic zone, the light-dark blue band the suboxic zone, the blue one the sulfidic zone, and
 222 the dark blue band the Ferruginous zone. Fe^{II} is the reduced iron part of aqueous Fe (Fe_F).

223 This ferruginous zone consists of anoxic conditions where Fe is mobilized as ferrous species
 224 (Fe^{II}), and was shown to be subsequently precipitated mainly as siderite and vivianite (Busigny

225 et al., 2016; Cosmidis et al., 2014; Poulton and Canfield, 2011; Viollier et al., 1997). Near the
 226 bottom, the nepheloid layer comprises strong elemental concentration gradients that reflect the
 227 upward diffusion of dissolved ions from the surficial sediment (Busigny et al., 2014).

228 3.2. Mercury speciation profiles

229 Total Hg concentrations in Lake Pavin waters are in the picomolar range, one order of
 230 magnitude higher than the ultra-trace oceanic concentration range (Bowman et al., 2020), but
 231 similar to other pseudo-pristine lakes, *i.e.*, lakes without local anthropogenic Hg inputs
 232 (Guédron et al., 2017; Leermakers et al., 1996; Regnell et al., 1997). THg_F ranged from 0.4 to
 233 8.8 pmol L^{-1} and THg_P from 0.4 to 4.6 pmol L^{-1} . Both THg_P and THg_F showed the lowest
 234 concentrations in the oxic mixolimnion and the highest ones in the mesolimnion (Fig. 4A).



235
 236 **Figure 4.** Depth concentration profiles of filtered (upper X-axis) and particulate (bottom X-axis)
 237 fractions (A) total Hg filtrated (THg_F), particulate (THg_P) and residual Hg ($\text{THg}_{F \text{ Res}} = \text{THg}_F - \text{MeHg}_F$),
 238 (B) ultra-filtered (THg_{UF}) and colloidal Hg (THg_{coll}), (C) dissolved gaseous Hg (DGM), and (D)
 239 methylmercury (MeHg). Corresponding redox zonation is also reported.

240 THg_P concentrations reached their maxima at 57 m, whereas THg_F maximum was found below,
 241 at 59 m. Then, they both show a progressive downward decrease in the sulfidic zone of the
 242 mesolimnion (Fig. 4A). In the mixolimnion, THg_F represented $\sim 50\%$ of THg (*i.e.*, $\text{THg}_P +$
 243 THg_F) and decreased abruptly to reach 27% at 55 m in the upper part of the suboxic zone of the

244 mesolimnion, followed by a gradual increase up to 75% at the bottom of this zone. Lateral
245 advection of Hg from underground water inputs (few liters per second) present at mid-depth in
246 the lake are negligible since a few measurements (data not shown) performed in the Goyon
247 spring (45°30'34.7" N; 2°54'15.6" E) waters indicated THg and MeHg concentrations at the
248 picomolar level. Below, in the sulfidic part of the mesolimnion, the proportion of the THg_F
249 increased gradually to reach an average percentage of 85% of THg. Within the filtered fraction,
250 the "truly dissolved" THg (THg_{UF}: 0.5-5.4 pmol L⁻¹) and colloidal part of the THg_F (THg_{coll} =
251 0.4-6.5 pmol L⁻¹) were quantitatively comparable. In the suboxic zone, THg_{coll} presented a sharp
252 peak at 59 m which dominated (i.e., 63 ± 15%) the THg_F fraction, and decreased in the sulfidic
253 zone (32 ± 9% of THg_F) to the benefit of THg_{UF} (Fig. 4B). Noteworthy is that the maxima of
254 the various THg fractions follow each other within a few meters between 57 and 60 m
255 deepening from particulate, colloidal, <0.45 μm, and truly dissolved. This suggests a
256 progressive dissolution of Hg downward.

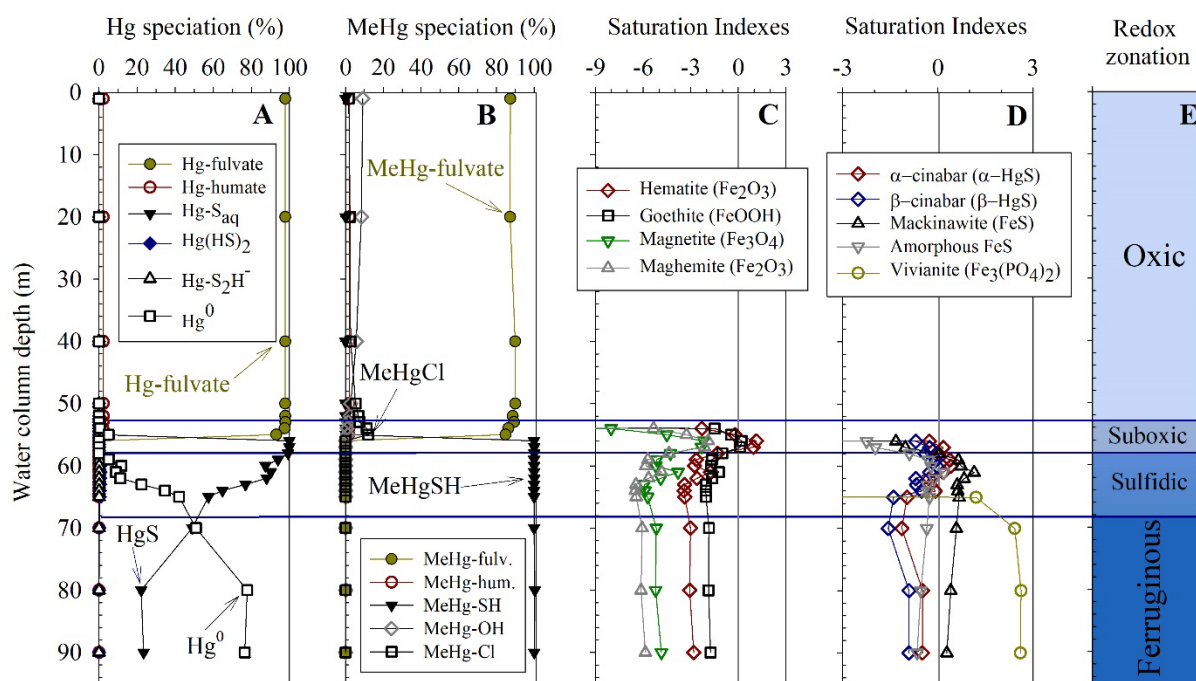
257 MeHg_F ranged from 0.03 to 6.8 pmol L⁻¹, whereas MeHg_P concentrations were two orders of
258 magnitude lower. Its distribution resembles the one of THg, with low concentration in the oxic
259 mixolimnion and higher ones in the anoxic monimolimnion, where it reaches up to 7.1 pmol L⁻¹
260 in the sulfidic zone of the lake (Fig. 4C). MeHg_P peaked at 57 m whereas MeHg_F showed a
261 broader maximum between 58 and 63 m (Fig. 4C). MeHg_F represented a minor fraction of THg_F
262 in the oxic mixolimnion (< 20%), and this proportion increased dramatically in the suboxic and
263 anoxic monimolimnion, reaching 90% between 62 and 70 m, and then decreased below 40% at
264 the bottom of the lake. Overall, MeHg_F, including the colloidal phase, is clearly the dominant
265 Hg species in the sulfidic zone. In contrast, MeHg_P never exceeded 10 % of the THg_P with the
266 highest proportions at 62 m.

267 Finally, DGM was between one and two order of magnitude lower than THg with the highest
268 concentrations found at the surface (0.26 pmol L⁻¹) and in the middle of the monimolimnion
269 (0.25 pmol L⁻¹ at 70 m, Fig. 4C).

270 **3.3 Crossed modeling using WHAM 7 and PHREEQC 2.0**

271 According to the thermodynamic calculations with WHAM 7 and PHREEQC 2.0, in the
272 mixolimnion, Hg and MeHg speciation is dominated by complexes with organic ligands (i.e.,
273 98% for Hg-FA and up to 87% MeHg-FA of the total MeHg) (Fig. 5 A and B). However, when
274 dissolved sulfide is present, in the sulfidic zone of the lake, complexes with sulfur ligands
275 dominate (i.e., > 65% of HgS and about 100% of MeHgSH). Calculated saturation indexes
276 indicated the saturation of iron oxides, mostly hematite (Fe₂O₃) and goethite (FeOOH), in the

277 suboxic part of the lake (Fig. 5C), whereas mineral phases of Fe, S, and P, including crystallized
 278 FeS (i.e., mackinawite) and vivianite ($\text{Fe}_3(\text{PO}_4)_2 \cdot 8\text{H}_2\text{O}$), are predicted to be saturated to over-
 279 saturated from the top of the sulfidic zone to the lake bottom (Fig. 5D).



280
 281 **Figure 5.** Modeled (A) Hg speciation (= THg-MeHg) including Hg^{II} and Hg^0 species, (B) MeHg
 282 speciation, and saturation indexes for (C) iron oxy(hydr)oxides and (D) sulfide and vivianite minerals
 283 (WHAM 7.0 and PHREEQC 2.0). Pyrrhotite saturation index was below -100 and is not presented in
 284 the figure. Corresponding redox zonation is also reported.

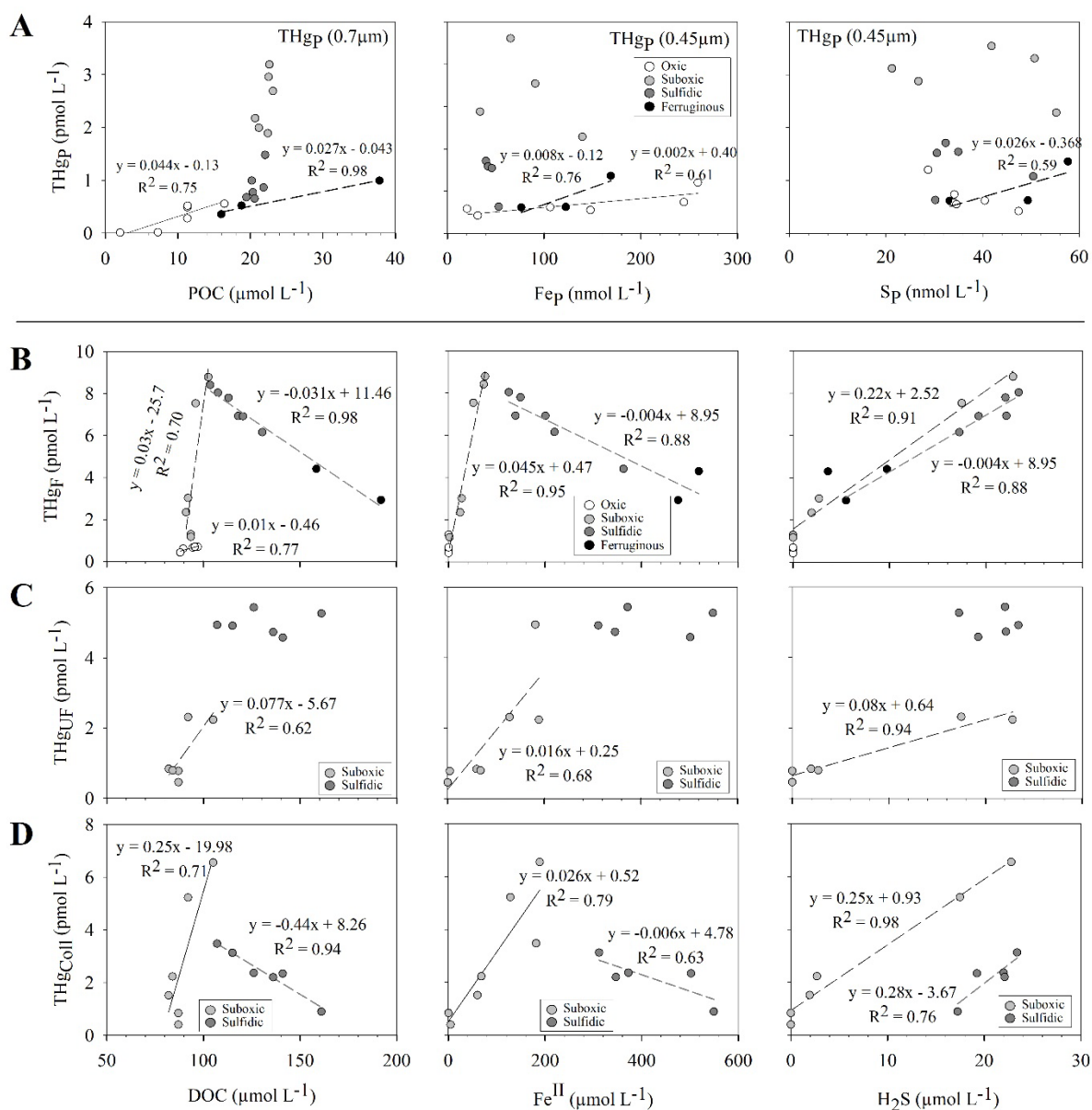
285 These results are consistent with previously published data (Bura-Nakic et al., 2009; Busigny
 286 et al., 2016; Jézéquel et al., 2016; Viollier et al., 1997). Interestingly, cinnabar (alpha and beta)
 287 minerals were found to be saturated in the upper part of the sulfidic zone (Fig. 5D), while all
 288 other Hg mineral species tested (Tab. SI.2), were found to be under-saturated.

289 4. DISCUSSION

290 4.1. Mercury carrier-phase exchanges along the redox gradient

291 In oxic waters, potential solid Hg carrier phases are limited due to the low mineralogical
 292 diversity of SPM in the upper part of Lake Pavin (Miot *et al.*, 2016). In surface waters, the
 293 biogenic particulate matter, mainly composed of diatoms and bacteria (Amblard and Bourdier,
 294 1990; Miot et al., 2016), constitutes the sink for atmospheric Hg deposited onto the surface of
 295 the lake. Known as the “biological pump” (Hain et al., 2014), this process is common for
 296 removing trace elements (including Hg) from surface waters of oceans and lakes, especially
 297 when it contains diatoms (Zaferani et al., 2018). This interpretation is supported by the positive
 298 relationship between THg_p and POC in the mixolimnion ($R^2 = 0.75$, Fig 6A). THg_p is also found

299 correlated with Fe_P ($R^2 = 0.90$, Fig 6A) which suggest a possible implication of the Fe oxides
 300 in the Hg-particulate organic matter (POM) consortiums. THg_F in the mixolimnion is also
 301 correlated with DOC (Fig. 6B), consistently with the predictions of our modeling, which shows
 302 that Hg-FA complexes dominate Hg species (98%) in the filtered phase (Fig. 5). The Hg-DOC
 303 association in natural waters is often thought to be the result of the high affinity of Hg for thiol
 304 functional groups of the DOC (Bouchet et al., 2018; Haitzer et al., 2002; Skjllberg et al., 2003).



305
 306 **Figure 6.** Total Mercury concentration in the A) the particulate (THg_P), B) the filtered ($THg_F < 0.45\mu$ m),
 307 C) the truly dissolved (THg_{UF}), and D) the colloidal (THg_{coll}) fractions versus organic carbon, iron and
 308 sulfide in the particulate (A) and filtered (B to D) fractions. Left panel of plot A reports particulate
 309 mercury (THg_P) and organic carbon (POC) obtained from the digestion of 0.7 μ m (GF/F) filters. Central
 310 and right panels report particulate mercury (THg_P), iron (Fe_P) and sulfur (S_P) concentrations obtained
 311 from the digestion of 0.45 μ m (PTFE) filters. All plotted regressions are significant and have p values
 312 below 0.05.

313 The vertical downward POM flux is slowed down when reaching the density gradient in the
314 mesolimnion and accumulated as indicated by the increase of THg, POC and SPM. There, POM
315 feeds the heterotrophic microorganisms, resulting in dissolved O₂ consumption as previously
316 described by Michard et al. (1994).

317 In the mesolimnion, no significant correlation was found between THg_P and POC, nor with
318 concentration of particulate Fe or S. This likely reflects the recycling of Hg onto successive
319 neoformed phases along the redox gradient (i.e., POC mineralization, reductive dissolution of
320 Mn and Fe oxy(hydr)oxides, Cf section 3.1). Changes in Hg carrier phases is particularly
321 evident in the filtered phase, as peaks in THg_F and MeHg_F occur below the onset of the decay
322 of both THg_P and MeHg_P, i.e., from the boundary between suboxic and sulfidic zone (Fig. 4).
323 Consistently with the recycling of POC and Mn or Fe oxides, both the truly dissolved Hg
324 (THg_{UF}) and the colloidal Hg (THg_{coll}) are found positively correlated with DOC, Fe^{II} and ΣH₂S
325 in the suboxic zone (Fig. 6 C and D). This confirms that the mineralization of POM and the
326 reductive dissolution of Fe-oxy(hydr)oxides below the oxycline have resulted in the release of
327 dissolved Hg and Fe^{II} (Hellal et al., 2015), and their redistribution in the filtered fraction, with
328 a dominance of Hg species bound to OM and/or FeS (i.e., mackinawite, Fig. 5D) colloids
329 (THg_{coll} = 63 ± 15% of THg_F). Below, in the sulfidic mesolimnion, our modeling predicted the
330 formation of both α- and β-cinnabar and FeS mineral phases (i.e., mackinawite and other
331 amorphous FeS phases, Fig. 5D) consistently with previous studies (Bura-Nakic et al., 2009).
332 In the filtered phase, truly dissolved THg (THg_{UF} = 68 ± 9% of THg_F) becomes dominant, and
333 is found independent of DOC, Fe^{II} and ΣH₂S (Fig. 6C). In contrast, THg_F and THg_{coll} are
334 inversely correlated with DOC and Fe^{II}, but positively correlated with ΣH₂S (Fig. 6 B and D).
335 This most probably illustrates the complex formation of Hg with sulfides in solution (i.e., HgS
336 nanoparticles and/or dissolved Hg-polysulfides) at the expense of OM complexation as
337 confirmed by our model (Figs. 5A, 5B), and consistently with colloidal HgS identified by
338 Energy dispersive X-ray spectrometry in deep-water of the Lake Pavin (Miot et al., 2016).
339 Although the thermodynamic modeling does not allow modeling colloidal HgS, the model
340 predicts the precipitation of HgS particles at the top of the sulfidic mesolimnion (Fig. 5D).
341 Hence, during the degradation of the POM in suboxic and anoxic conditions, the nature of the
342 particulate Hg-OM binding sites change, favoring the preferential binding of Hg to stronger
343 dissolved ligands, such as thiol groups of the FA (Bouchet et al., 2018; Feyte et al., 2012; Liang
344 et al., 2019) and the formation of FeS and HgS colloids in the dissolved phase, which is at
345 equilibrium with HgS minerals.

346 In the ferruginous monimolimnion, although the number of observations is limited ($n = 3$),
347 THg_P rise with rising POC, Fe_P and S_P concentrations (Fig. 6A). This is consistent with an
348 association of Hg with both iron sulfides, and/or sulfidized OM, consistent with the predictions
349 of the model. It is however important to recall that this area is the most devoid of particulate
350 Hg. In this ferruginous zone, Fe_P and P_P covary ($R^2 = 0.95$, $n = 3$, $p < 0.10$), with 1.5 mole of Fe
351 per mole of P, supporting the presence of vivianite as already identified in deep waters of Lake
352 Pavin (Busigny et al., 2016; Cosmidis et al., 2014) and confirmed by our thermodynamic
353 modeling (Fig. 5D). It is thus probable that such Fe-phosphates precipitates together with other
354 FeS minerals, in association with bacteria (Miot et al., 2016) or diatoms (i.e., THg_P vs Si_P , $R^2 =$
355 0.64 , $n = 6$, $p < 0.05$), could favor the scavenging and export of Hg to the sediment of Lake
356 Pavin. In brief, the Hg-OM partition appears to be involved in the Fe-S redox and partition
357 changes known as the “iron-wheel” of the Lake Pavin (Busigny et al., 2016; Viollier et al.,
358 1997).

359 **4.2. Mercury methylation/demethylation**

360 MeHg in Lake Pavin is in similar proportions as in other meromictic lakes or artificial reservoirs
361 in various lakes around the world (Peretyazhko et al., 2006b; Watras and Bloom, 1994). In the
362 Great Salt Lake, the Petit-Saut reservoir, and Wisconsin or Canadian lakes, all stratified with
363 an anoxic hypolimnion, comparable MeHg distribution patterns have been observed resulting
364 from increased net Hg methylation in the lake bottom waters (Acha et al., 2012; Eckley et al.,
365 2005; Eckley and Hintelmann, 2006; Muresan et al., 2008; Porcella, 1994; Regnell et al., 1997;
366 Regnell and Tunlid, 1991; Watras and Bloom, 1994; Yang et al., 2020). The same is true for
367 marine environments where meromixis occurs (e.g., Black Sea and the Baltic Sea), resulting in
368 high MeHg in their anoxic waters (Pempkowiak et al., 1998; Rosati et al., 2018; Soerensen et
369 al., 2018).

370 In Lake Pavin, MeHg is strongly correlated with THg both in the filtered phase ($R^2 = 0.92$, $n =$
371 21 , $p < 0.01$), and in the particulate phase ($R^2 = 0.85$, $n = 21$, $p < 0.01$). In the monimolimnion,
372 MeHg constitutes the main fraction of the THg (i.e., 77 ± 22 % of the THg_F , and 71 ± 24 % of
373 the THg_P). MeHg_F is highly correlated with $\Sigma\text{H}_2\text{S}$ ($R^2 = 0.96$, $n = 20$, $p < 0.01$) along the entire
374 water column. The onset of MeHg accumulation occurs in the suboxic zone, and reaches a
375 plateau in the sulfidic layer where $\Sigma\text{H}_2\text{S}$ and Fe^{II} are the most intensively produced. The steepest
376 MeHg_F gradient is located between 57 and 58 m (Fig. 4D), at the same depth as the steepest
377 $\text{SO}_4/\Sigma\text{H}_2\text{S}$ drops (Figs. 3D and 3E). This feature indicates that MeHg is dominantly produced
378 by methylating-SRB, a group of strains reported owning the methylating *hgc* gene (Paranjape

379 and Hall, 2017; Regnell and Watras, 2018). SRB account for a large part of the bacteria in the
380 entire monimolimnion of Lake Pavin (Berg et al., 2019; Lehours et al., 2016). The presence of
381 high MeHg_F and THg_{UF} ($R^2 = 0.84$, $n = 12$, $p < 0.01$) concentrations in the sulfidic zone (Fig.
382 4B, 4D) strongly suggests that HgS complexes, neutral Hg polysulfides, and possibly Hg-
383 thiolates (Fig. 5A, 5B), are abundant enough to constitute substrates for Hg methylation by SRB
384 as suggested in several experiments or modeling (Benoit et al., 1999; Schaefer and Morel, 2009;
385 Skyllberg, 2008). On the other hand, several strains can demethylate MeHg under anoxic
386 conditions including SRB and methanogens (Bridou et al., 2011; Oremland et al., 1991). The
387 decrease in MeHg_F concentrations in the ferruginous zone is coincident with the increase in
388 DGM, which supports the hypothesis of reductive demethylation in the Lake bottom. However,
389 the amount of produced DGM could only explain a small fraction (i.e. <5-10%) of the decrease
390 of MeHg_F observed, suggesting that significant proportion of MeHg_F is also likely exported to
391 the sediment in association neoformed FeS minerals (see paragraph 5.1.).

392 **4.3. Mercury reduction**

393 The DGM concentration profile in the Lake Pavin waters column exhibits high levels in surface
394 waters and at 70 m in the anoxic monimolimnion (Fig. 4C). No trace of dimethylmercury was
395 found in the samples, consistently with previous results (Cossa et al., 1994), suggesting that
396 DGM consists entirely of Hg⁰. The high DGM measured in surface waters suggests that Hg⁰ is
397 formed *via* Hg^{II} photoreduction in the euphotic zone, and is partially reinjected in the
398 atmosphere as already shown in numerous lakes (Amyot et al., 1994; Guédron et al., 2020a;
399 Saiz-Lopez et al., 2018). In contrast, the presence of DGM peaks in the aphotic monimolimnion
400 supports non-photochemical processes for DGM production, such as Hg^{II} microbial reduction
401 (Lamborg et al., 2013; Mason et al., 1995; Rolfhus and Fitzgerald, 2004) and/or natural OM-
402 mediated reduction of Hg^{II} (Allard and Arsenie, 1991; Zheng et al., 2011). Hg⁰ is consistently
403 predicted by the model, increasing from the sulfidic mesolimnion to the ferruginous
404 monimolimnion (Fig. 5A). The large proportion of truly dissolved Hg (i.e., 59 and 81% of
405 THg_F) possibly bound to labile organic molecules could favor its reduction by natural OM (Gu
406 et al., 2011; Zheng et al., 2011). Alternatively, the abiotic reduction of Hg^{II} to Hg⁰ could also
407 be induced by Fe^{II} in the presence of Fe-oxy(hydr)oxides (Charlet et al., 2002; Peretyazhko et
408 al., 2006a), such as hematite reported from 70 m down to 86 m in the Pavin Lake (Cosmidis et
409 al., 2014). Hg reduction in the presence of nanoparticulate vivianite has also recently been
410 demonstrated in anoxic circumneutral pH water (Etique et al., 2021). Also, the reduction of
411 Hg^{II}-S^{-II} complexes by FeS to Hg⁰ is thermodynamically possible (Bone et al., 2014) at Eh

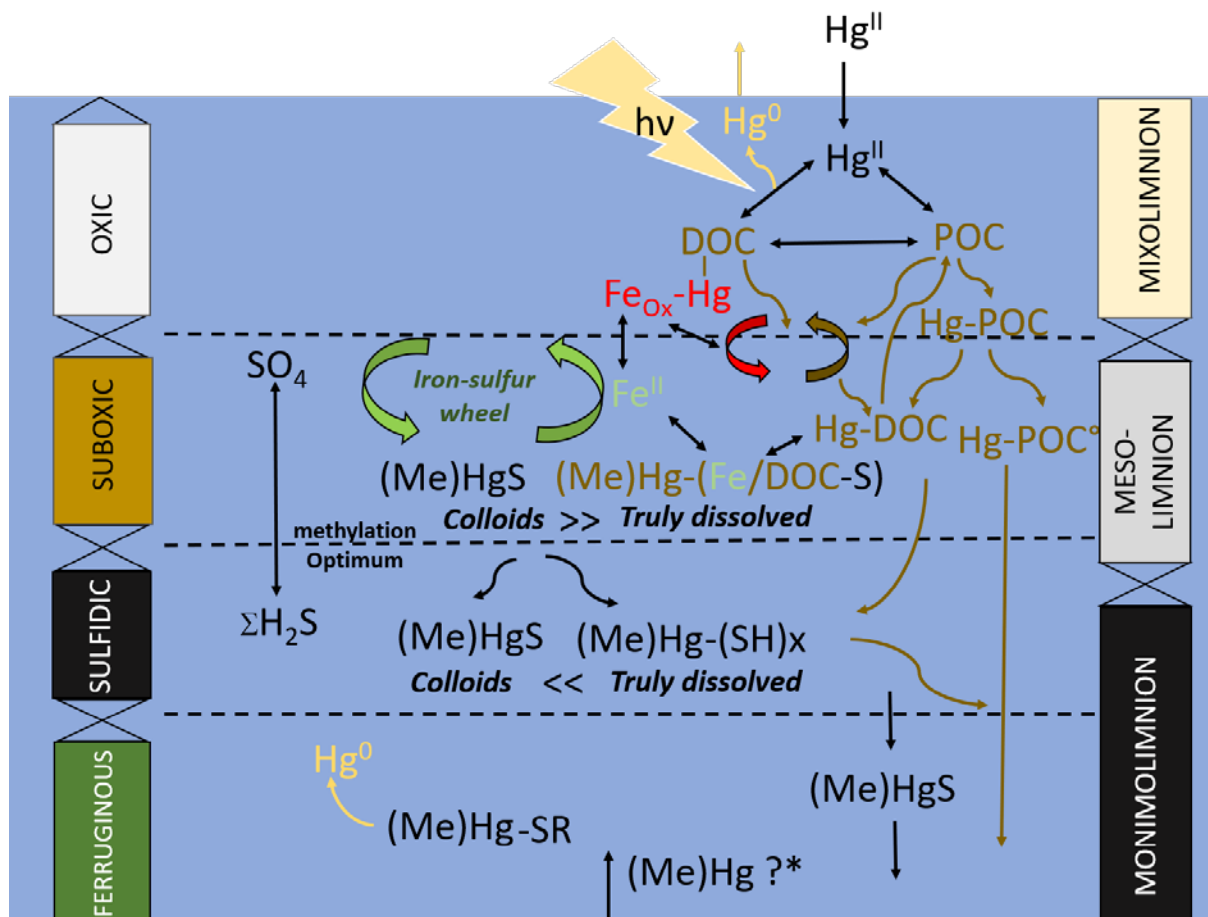
412 values in the range of Lake Pavin waters below 59 m. However, the occurrence of DGM peaks
413 in the monimolimnion in phase with decreasing MeHg concentrations (Fig. 4) also supports the
414 hypothesis of reductive MeHg demethylation with the production of Hg^0 and CH_4 (Aeschbach-
415 Hertig et al., 1999). Reductive demethylation is the fact of *Geobacter* sp. (Lu et al., 2016), some
416 of them identified in Lake Pavin waters (Berg et al., 2019). In summary, under the current
417 observations of Pavin waters, it is not possible to sort out the actual reactions involved in the
418 reducing process that produce the DGM in the monimolimnion. In the present state, we cannot
419 explain the difference between the measured and model-derived DGM concentrations. An in-
420 depth study with higher resolution lake bottom profiles together with experimental works are
421 required to solve this issue.

422 5. SYNTHESIS AND CONCLUSIONS

423 The high-resolution observation and modeling of Hg speciation and partition at the redox
424 interfaces of Lake Pavin allow the proposal of a conceptual biogeochemical behavior of Hg
425 which can be typical of other meromictic ferruginous lakes (Fig. 7). Because it has a very small
426 catchment area that minimizes Hg inputs from the drainage basin, Lake Pavin receives Hg
427 mainly from the atmosphere. Once deposited onto surface waters, a part of Hg is photo-reduced
428 and reinjected in the atmosphere, whereas another part binds to DOC and sorbs onto biogenic
429 particulate matter produced in the euphotic zone and conveyed at depth by settling POC, in a
430 process known as “biological pumping”.

431 The Hg associated with POM accumulates where the conductivity gradient generates a strong
432 stratification. There, the mineralization of OM occurs, consuming dissolved oxygen and
433 generating a suboxic zone, causing the mobilization of a fraction of Hg. Mercury diffuses up
434 and down from this Hg-enriched zone. On its way up, Hg adsorbs onto Fe-oxy(hydr)oxides
435 (associated with POM) that precipitated on the top of the oxycline; on its way down, Hg diffuses
436 as truly-dissolved and colloidal HgS species and partly precipitate as HgS minerals.
437 Simultaneously, in this suboxic zone, available Hg^{II} is methylated by SRB. Deeper in the anoxic
438 monimolimnion, sulfidation favors the formation of dissolved Hg fraction and possibly the
439 reductive demethylation of MeHg with Hg^0 production. A part of the Hg and MeHg produced
440 in the suboxic and sulfidic zone is also likely exported to the sediment with settling particles.
441 In brief, the “biological pump”, the “iron-sulfur wheel”, through associated bacteria consortia,
442 control the Hg cycling in the Pavin waters. This behavior is in line with already existing
443 biogeochemical models and allows us to observe the already identified homogenous and
444 heterogeneous reactions and processes along a single water column covering the entire redox

445 range of natural waters. More detailed observations on the Hg speciation in the ferruginous
 446 monimolimnion are needed to evaluate the possible effect of Hg input from hydrothermal and
 447 diffusive inputs at the bottom of the lake in addition to quantitative export fluxes and reaction
 448 rates within the lake.



449
 450 **Figure 7.** Conceptual model for the Hg and MeHg cycle in Lake Pavin with the recycling of organic
 451 matter, sulfur, and iron. (Me)Hg refers to both MeHg and Hg species, ticks (-) indicate the binding
 452 with particulate carrier phases (i.e., iron oxides (Fe_{ox}), particulate organic carbon (POC) and iron
 453 sulfides (FeS) or binding with aqueous ligands (i.e., dissolved organic carbon (DOC), free or DOC
 454 polysulfides (SR). $Hg-POC^{\circ}$ considers Hg bound to both particles and microbial cells. (Me)Hg* refers
 455 to possible upward release of MeHg and THg from the sediment.

456

457 **Acknowledgments**

458 All chemical analyses have been performed at the *Geochemistry & Mineralogy* platform of
459 ISTERre (Université Grenoble Alpes, France), except for particulate organic carbon that has
460 been determined at the analytical platform of the Mediterranean Institute of Oceanography
461 (MIO, Université Aix-Marseille, France), and anions that have been determined at the Air-o-
462 sol analytical platform of the Institute of Environmental Geosciences (IGE, Université
463 Grenoble Alpes, France). This work is a contribution to the PALMERLAC project supported
464 by a grant from Labex OSUG@2020 (PI: D. Cossa and D. Tisserand). D. Cossa, D. Tisserand,
465 and S. Guédron (ISTERre/IRD/UGA) are part of Labex OSUG@2020 (Investissements d'avenir
466 ANR10 LABX56). The authors thank the City of Besse-et-Saint-Anastaise and the members of
467 the Station Biologique de Besse (Université Clermont Auvergne), especially Corinne Mesta for
468 logistical supports during field campaigns, and colleagues from IPGP and IMPMC for their
469 help during sampling.

470

471 **Terminology of mercury chemical species:**

472 THg : Total Hg (all Hg species);

473 MMHg : Monomethyl Hg;

474 DMHg : Dimethyl Hg;

475 MeHg : Methylated Hg (MeHg = MMHg + DMHg);

476 Hg⁰ : Elemental Hg;

477 Hg^{II} : Divalent Hg;

478 DGM : Dissolved Gaseous Hg (DGM = Hg⁰ + DMHg);

479 THg_F : Total Hg in filtrated (0.45 μm);

480 THg_P : Total particulate Hg (>0.45μm);

481 MeHg_F : Methylated Hg in filtrated (0.45 μm);

482 MeHg_P : Methylated particulate Hg (>0.45μm);

483 THg_{UF} : Truly dissolved Hg, *i.e.*, ultrafiltered samples (< 3 kDa);

484 THg_{coll} : Colloidal Hg, *i.e.*, fraction > 3 kDa and < 0.45 μm;

485 THg_{F Res} : THg_F - MeHg_F;

486 THg_{P Res} : THg_P - MeHg_P.

487

REFERENCES

- 489 Achá, D., Pabon, C.A., Hintelmann, H., 2012. Mercury methylation and hydrogen sulfide
490 production among unexpected strains isolated from periphyton of two macrophytes of the
491 Amazon. *FEMS microbiology ecology* 80, 637-645.
- 492 Aeschbach-Hertig, W., Hofer, M., Kipfer, R., Imboden, D., Wieler, R., 1999. Accumulation of
493 mantle gases in a permanently stratified volcanic Lake (Lac Pavin, France). *Geochimica et*
494 *Cosmochimica Acta* 63, 3357-3372.
- 495 Amblard, C., Bourdier, G., 1990. The spring bloom of the diatom *Melosira italica* subsp.
496 *subarctica* in Lake Pavin: biochemical, energetic and metabolic aspects during sedimentation.
497 *Journal of Plankton Research* 12, 645-660.
- 498 Amyot, M., McQueen, D.J., Mierle, G., Lean, D.R.S., 1994. Sunlight-Induced Formation of
499 Dissolved Gaseous Mercury in Lake Waters. *Environmental science & technology* 28, 2366-
500 2371.
- 501 Barone, V., Bencini, A., Totti, F., Uytterhoeven, M.G., 1996. Theoretical Characterization of
502 the Mechanism of Hg–C Bond Cleavage by Halogenic Acids. *Organometallics* 15, 1465-1469.
- 503 Benoit, J., Gilmour, C., Mason, R., Heyes, A., 1999. Sulfide controls on mercury speciation
504 and bioavailability to methylating bacteria in sediment pore waters. *Environ. Sci. Technol.* 33,
505 951-957.
- 506 Berg, J.S., Jézéquel, D., Duverger, A., Lamy, D., Laberty-Robert, C., Miot, J., 2019. Microbial
507 diversity involved in iron and cryptic sulfur cycling in the ferruginous, low-sulfate waters of
508 Lake Pavin. *PLoS One* 14, e0212787.
- 509 Blanc, P., Burnol, A., Marty, N., Hellal, J., Guérin, V., Laperche, V., 2018. Methylmercury
510 complexes: Selection of thermodynamic properties and application to the modelling of a
511 column experiment. *Science of the Total Environment* 621, 368-375.
- 512 Bloom, N., 1996. Method 1613 Mercury in water by oxidation, purge, and trap, and CVAFS,
513 Washington.
- 514 Bone, S.E., Bargar, J.R., Sposito, G., 2014. Mackinawite (FeS) reduces mercury (II) under
515 sulfidic conditions. *Environmental science & technology* 48, 10681-10689.
- 516 Bonhomme, C., Jézéquel, D., Poulin, M., Saad, M., Vinçon-Leite, B., Tassin, B., 2016. Lake
517 Pavin mixing: new insights from high resolution continuous measurements, Lake Pavin.
518 Springer, pp. 177-184.
- 519 Bonhomme, C., Poulin, M., Vinçon-Leite, B., Saad, M., Groleau, A., Jézéquel, D., Tassin, B.,
520 2011. Maintaining meromixis in Lake Pavin (Auvergne, France): the key role of a sublacustrine
521 spring. *Comptes Rendus Geoscience* 343, 749-759.

522 Bouchet, S., Goni-Urriza, M., Monperrus, M., Guyoneaud, R., Fernandez, P., Heredia, C.,
523 Tessier, E., Gassie, C., Point, D., Guédron, S., Acha, D., Amouroux, D., 2018. Linking
524 microbial activities and low molecular weight thiols to Hg methylation in biofilms and
525 periphyton from high altitude tropical lakes (Bolivian altiplano). *Environmental science &*
526 *technology* 52, 9758-9767.

527 Bowman, K.L., Lamborg, C.H., Agather, A.M., 2020. A global perspective on mercury cycling
528 in the ocean. *Science of The Total Environment* 710, 136166.

529 Bridou, R., Monperrus, M., Gonzalez, P.R., Guyoneaud, R., Amouroux, D., 2011.
530 Simultaneous determination of mercury methylation and demethylation capacities of various
531 sulfate-reducing bacteria using species-specific isotopic tracers. *Environmental toxicology and*
532 *chemistry* 30, 337-344.

533 Buffle, J., Chalmers, R.A., 1988. *Complexation reactions in aquatic systems*. Chichester.

534 Bura-Nakic, E., Viollier, E., Jézéquel, D., Thiam, A., Ciglenecki, I., 2009. Reduced sulfur and
535 iron species in anoxic water column of meromictic crater Lake Pavin (Massif Central, France).
536 *Chemical Geology* 266, 311-317.

537 Busigny, V., Jézéquel, D., Cosmidis, J., Viollier, E., Benzerara, K., Planavsky, N.J., Albéric,
538 P., Lebeau, O., Sarazin, G., Michard, G., 2016. The iron wheel in lac Pavin: interaction with
539 phosphorus cycle, Lake Pavin. Springer, pp. 205-220.

540 Busigny, V., Planavsky, N.J., Jézéquel, D., Crowe, S., Louvat, P., Moureau, J., Viollier, E.,
541 Lyons, T.W., 2014. Iron isotopes in an Archean ocean analogue. *Geochimica et Cosmochimica*
542 *Acta* 133, 443-462.

543 Chapron, E., Albéric, P., Jézéquel, D., Versteeg, W., Bourdier, J.-L., Sitbon, J., 2010.
544 Multidisciplinary characterisation of sedimentary processes in a recent maar lake (Lake Pavin,
545 French Massif Central) and implication for natural hazards. *Natural Hazards and Earth System*
546 *Sciences* 10, 1815-1827.

547 Charlet, L., Bosbach, D., Peretyashko, T., 2002. Natural attenuation of TCE, AS, Hg linked to
548 the heterogeneous oxidation of Fe (II) : an AFM study. *Chem. Geol.*

549 Cline, J.D., 1969. Spectrophotometric determination of hydrogen sulfide in natural waters 1.
550 *Limnology and Oceanography* 14, 454-458.

551 Cooper, C.J., Zheng, K., Rush, K.W., Johs, A., Sanders, B.C., Pavlopoulos, G.A., Kyrpides,
552 N.C., Podar, M., Ovchinnikov, S., Ragsdale, S.W., Parks, J.M., 2020. Structure determination
553 of the HgcAB complex using metagenome sequence data: insights into microbial mercury
554 methylation. *Communications Biology* 3, 320.

555 Cosmidis, J., Benzerara, K., Morin, G., Busigny, V., Lebeau, O., Jézéquel, D., Noël, V., Dublet,
556 G., Othmane, G., 2014. Biomineralization of iron-phosphates in the water column of Lake
557 Pavin (Massif Central, France). *Geochimica et Cosmochimica Acta* 126, 78-96.

558 Cossa, D., Averty, B., Bretaudeau, J., Senard, A.S., 2003. Dissolved mercury speciation in
559 marine waters. *Analysis methods in marine environment*. Ifremer and French Ministry of
560 Sustainable Development and Ecology (in French).

561 Cossa, D., Coquery, M., 2005. The mediterranean mercury anomaly, a geochemical or a
562 biological issue. *The Mediterranean Sea*, 177-208.

563 Cossa, D., de Madron, X.D., Schaefer, J., Guédron, S., Maruszczak, N., Castelle, S., Naudin, J.-
564 J., 2017. Sources and exchanges of mercury in the waters of the Northwestern Mediterranean
565 margin. *Progress in Oceanography*.

566 Cossa, D., Gobeil, C., 2000. Mercury speciation in the Lower St. Lawrence estuary. *Can. J.*
567 *Fish. Aquat. Sci.* 57, 138-147.

568 Cossa, D., Mason, R.P., Fitzgerald, W.F., 1994. Chemical speciation of mercury in a
569 Meromictic lake, in: J., W.C., W., H.J. (Eds.), *Mercury pollution: integration and synthesis*.
570 CRC Press, Inc., pp. 57-67.

571 Drott, A., Björn, E., Bouchet, S., Skyllberg, U., 2013. Refining Thermodynamic Constants for
572 Mercury(II)-Sulfides in Equilibrium with Metacinnabar at Sub-Micromolar Aqueous Sulfide
573 Concentrations. *Environmental science & technology* 47, 4197-4203.

574 Dyrssen, D., Wedborg, M., 1991. The sulphur-mercury(II) system in natural waters. *Water, air*
575 *and soil pollution*. 56, 507-519.

576 Eckley, C., Watras, C., Hintelmann, H., Morrison, K., Kent, A., Regnell, O., 2005. Mercury
577 methylation in the hypolimnetic waters of lakes with and without connection to wetlands in
578 northern Wisconsin. *Canadian Journal of Fisheries and Aquatic Sciences* 62, 400-411.

579 Eckley, C.S., Hintelmann, H., 2006. Determination of mercury methylation potentials in the
580 water column of lakes across Canada. *Science of the Total Environment* 368, 111-125.

581 Etique, M., Bouchet, S., Byrne, J.M., ThomasArrigo, L.K., Kaegi, R., Kretzschmar, R., 2021.
582 Mercury Reduction by Nanoparticulate Vivianite. *Environmental Science & Technology*.

583 Feyte, S., Gobeil, C., Tessier, A., Cossa, D., 2012. Mercury dynamics in lake sediments.
584 *Geochimica et Cosmochimica Acta* 82, 92-112.

585 Feyte, S., Tessier, A., Gobeil, C., Cossa, D., 2010. In situ adsorption of mercury, methylmercury
586 and other elements by iron oxyhydroxides and organic matter in lake sediments. *Applied*
587 *Geochemistry* 25, 984-995.

588 Fitzgerald, W.F., Lamborg, C.H., Turekian, H.D., Holland, K.K., 2014. 11.4 - Geochemistry of
589 Mercury in the Environment, Treatise on Geochemistry (Second Edition). Elsevier, Oxford, pp.
590 91-129.

591 Froelich, P.N., Klinhammer, G.P., Bender, M.L., Luedtke, N.A., Heath, G.R., Cullen, D.,
592 Dauphin, P., Hammond, D., Hartman, B., Maynard, V., 1979. Early oxidation of organic matter
593 in pelagic sediments of the eastern equatorial atlantic: suboxic diagenesis. *Geochemica et*
594 *cosmochemica Acta* 43, 1075-1090.

595 Gobeil, C., Cossa, D., 1993. Mercury in sediments and sediment pore water in the Laurential
596 Trough. *Can. J. Fish. Aquat.Sci.* 50, 1794-1880.

597 Gu, B., Bian, Y., Miller, C.L., Dong, W., Jiang, X., Liang, L., 2011. Mercury reduction and
598 complexation by natural organic matter in anoxic environments. *Proceedings of the National*
599 *Academy of Sciences* 108, 1479-1483.

600 Guédron, S., Achá, D., Bouchet, S., Point, D., Tessier, E., Heredia, C., Rocha-Lupa, S.,
601 Fernandez-Saavedra, P., Flores, M., Bureau, S., 2020a. Accumulation of Methylmercury in the
602 High-Altitude Lake Uru Uru (3686 m asl, Bolivia) Controlled by Sediment Efflux and
603 Photodegradation. *Applied Sciences* 10, 7936.

604 Guédron, S., Audry, S., Acha, D., Bouchet, S., Point, D., Condom, T., Heredia, C., Campillo,
605 S., Baya, P.A., Groleau, A., Amice, E., Amouroux, D., 2020b. Diagenetic production,
606 accumulation and sediment-water exchanges of methylmercury in contrasted sediment facies
607 of Lake Titicaca (Bolivia). *Science of the total environment* 723, 138088.

608 Guédron, S., Devin, S., Vignati, D.A.L., 2016. Total and methylmercury partitioning between
609 colloids and true solution: From case studies in sediment overlying and porewaters to a
610 generalized model. *Environmental Toxicology and Chemistry* 35, 330-339.

611 Guédron, S., Grimaldi, M., Grimaldi, C., Cossa, D., Tisserand, D., Charlet, L., 2011.
612 Amazonian former gold mined soils as a source of methylmercury: Evidence from a small scale
613 watershed in French Guiana. *Wat. Res.* 45, 2659-2669.

614 Guédron, S., Point, D., Acha, D., Bouchet, S., Baya, P.A., Molina, C.I., Tessier, E., Monperrus,
615 M., Flores, M., Fernandez Saavedra, P., Espinoza, M.E., Heredia, C., Rocha, S., Groleau, A.,
616 Amice, E., Thebault, J., Alanoca, L., Duwig, C., Uzu, G., Lazzaro, X., Bertrand, A., Bertrand,
617 S., Barbaud, C., Gibon, F.M., Ibanez, C., Zepita, C., Chauvaud, L., Amouroux, D., 2017.
618 Mercury contamination level and speciation inventory in the hydrosystem of Lake Titicaca:
619 current status and future trends. *Environmental Pollution* 231, 262-270.

620 Hain, M.P., Sigman, D., Haug, G., 2014. 8.18–The biological Pump in the Past. Reference
621 Module in Earth Systems and Environmental Sciences, Treatise on Geochemistry (Second
622 Edition), The Oceans and Marine Geochemistry 8, 485-517.

623 Haitzer, M., Aiken, G.R., Ryan, J.N., 2002. Binding of mercury(II) to dissolved organic matter:
624 the role of the mercury-to-DOM concentration ratio. *Environ. Sci. Technol.* 36, 3564–3570.

625 Hellal, J., Guédron, S., Huguet, L., Schaefer, J., Laperche, V., Joulian, C., Lanceleur, L.,
626 Burnol, A., Ghestem, J.-P., Garrido, F., Battaglia-Brunet, F., 2015. Mercury mobilization and
627 speciation linked to bacterial iron oxide and sulfate reduction: A column study to mimic reactive
628 transfer in an anoxic aquifer. *Journal of Contaminant Hydrology* 180, 56-68.

629 Iverfeldt, Å., 1988. Mercury in the Norwegian fjord Framvaren. *Marine Chemistry* 23, 441-
630 456.

631 Jeong, H.Y., Klaue, B., Blum, J.D., Hayes, K.F., 2007. Sorption of mercuric ion by synthetic
632 nanocrystalline mackinawite (FeS). *Environmental science & technology* 41, 7699-7705.

633 Jézéquel, D., Michard, G., Viollier, E., Agrinier, P., Albéric, P., Lopes, F., Abril, G.,
634 Bergonzini, L., 2016. Carbon cycle in a meromictic crater lake: Lake Pavin, France, Lake Pavin.
635 Springer, pp. 185-203.

636 Juvigné, E., Bastin, B., Delibrias, G., Evin, J., Gewalt, M., Gilot, E., Streeel, M., 1996. A
637 comprehensive pollen-and tephra-based chronostratigraphic model for the Late Glacial and
638 Holocene period in the French Massif Central. *Quaternary International* 34, 113-120.

639 Kim, C., Rytuba, J.J., Brown, J.G.E., 2004. EXAFS study of mercury (II) sorption to Fe- and
640 Al- (hydr)oxides I. Effect of pH. *J. Colloid Interface Sci.* 271, 1-15.

641 Lamborg, C.H., Kent, D.B., Swarr, G.J., Munson, K.M., Kading, T., O'Connor, A.E., Fairchild,
642 G.M., LeBlanc, D.R., Wiatrowski, H.A., 2013. Mercury Speciation and Mobilization in a
643 Wastewater-Contaminated Groundwater Plume. *Environmental science & technology* 47,
644 13239-13249.

645 Lamborg, C.H., Yigiterhan, O., Fitzgerald, W.F., Balcom, P.H., Hammerschmidt, C.R.,
646 Murray, J., 2008. Vertical distribution of mercury species at two sites in the Western Black Sea.
647 *Mar. Chem.* 111, 77-89.

648 Leermakers, M., Meuleman, C., Baeyens, W., 1996. Mercury distribution and fluxes in Lake
649 Baikal, Global and regional mercury cycles: Sources, fluxes and mass balances. Springer, pp.
650 303-315.

651 Lehours, A.-C., Borrel, G., Morel-Desrosiers, N., Bardot, C., Grossi, V., Keraval, B., Attard,
652 E., Morel, J.-P., Amblard, C., Fonty, G., 2016. Anaerobic Microbial Communities and

653 Processes Involved in the Methane Cycle in Freshwater Lakes—a Focus on Lake Pavin, Lake
654 Pavin. Springer, pp. 255-284.

655 Liang, X., Lu, X., Zhao, J., Liang, L., Zeng, E.Y., Gu, B., 2019. Stepwise reduction approach
656 reveals mercury competitive binding and exchange reactions within natural organic matter and
657 mixed organic ligands. *Environmental Science & Technology* 53, 10685-10694.

658 Loux, N.T., 1998. An assessment of mercury-species-dependent binding with natural organic
659 carbon. *Chemical Speciation & Bioavailability* 10, 127-136.

660 Lu, X., Liu, Y., Johs, A., Zhao, L., Wang, T., Yang, Z., Lin, H., Elias, D.A., Pierce, E.M., Liang,
661 L., 2016. Anaerobic mercury methylation and demethylation by *Geobacter bemidjiensis* Bem.
662 *Environmental science & technology* 50, 4366-4373.

663 Malcolm, R., 1985. Geochemistry of stream fulvic and humic substances. *Humic substances in*
664 *soil, sediment, and water: geochemistry, isolation and characterization*, 181-209.

665 Martin, J.-M., 1985. Pavin Crater Lake. *Chemical Processes in Lakes*, John Wiley and Sons,
666 New York New York. 1985. p 169-188, 11 fig, 2 tab, 50 ref.

667 Mason, R., Lawson, N., Lawrence, A., Leaner, J., Lee, J., Sheu, G.-R., 1999. mercury in the
668 Chesapeake Bay. *Marine Chemistry* 65, 77-96.

669 Mason, R., Morel, F.a., Hemond, H., 1995. The role of microorganisms in elemental mercury
670 formation in natural waters. *Water, Air, and Soil Pollution* 80, 775-787.

671 Mason, R.P., Choi, A.L., Fitzgerald, W.F., Hammerschmidt, C.R., Lamborg, C.H., Soerensen,
672 A.L., Sunderland, E.M., 2012. Mercury biogeochemical cycling in the ocean and policy
673 implications. *Environmental Research* 119, 101-117.

674 Mercone, D., Thomson, J., Croudace, I., Troelstra, S., 1999. A coupled natural immobilisation
675 mechanism for mercury and selenium in deep-sea sediments. *Geochimica et Cosmochimica*
676 *Acta* 63, 1481-1488.

677 Merritt, K.A., Amirbahman, A., 2007. Mercury dynamics in sulfide-rich sediments:
678 Geochemical influence on contaminant mobilization within the Penobscot River estuary,
679 Maine, USA. *Geochimica et Cosmochimica Acta* 71, 929-941.

680 Michard, G., Viollier, E., Jézéquel, D., Sarazin, G., 1994. Geochemical study of a crater lake:
681 Pavin Lake, France—Identification, location and quantification of the chemical reactions in the
682 lake. *Chemical Geology* 115, 103-115.

683 Miot, J., Jézéquel, D., Benzerara, K., Cordier, L., Rivas-Lamelo, S., Skouri-Panet, F., Férard,
684 C., Poinot, M., Duprat, E., 2016. Mineralogical diversity in Lake Pavin: connections with
685 water column chemistry and biomineralization processes. *Minerals* 6, 24.

686 Muresan, B., Cossa, D., Coquery, M., Richard, S., 2008. Mercury sources and transformations
687 in a man-perturbed tidal estuary: The Sinnamary Estuary, French Guiana. *Geochim.*
688 *Cosmochim. Acta* 72, 5416-5430.

689 Muresan, B., Metzger, É., Jézéquel, D., Cossa, D., 2018. A multiscale study of mercury
690 transformations and dynamics at the chemocline of the Petit-Saut tropical reservoir (French
691 Guiana). *Science of the Total Environment* 630, 1401-1412.

692 Oremland, R.S., Culbertson, C.W., Winfrey, M.R., 1991. Methylmercury decomposition in
693 sediments and bacterial cultures: involvement of methanogens and sulfate reducers in oxidative
694 demethylation. *Applied and environmental microbiology* 57, 130-137.

695 Paranjape, A.R., Hall, B.D., 2017. Recent advances in the study of mercury methylation in
696 aquatic systems. *Facets* 2, 85-119.

697 Parkhurst, D.L., Appelo, C., 2013. Description of input and examples for PHREEQC version
698 3—a computer program for speciation, batch-reaction, one-dimensional transport, and inverse
699 geochemical calculations. *US geological survey techniques and methods* 6, 497.

700 Parks, J.M., Johs, A., Podar, M., Bridou, R., Hurt, R.A., Smith, S.D., Tomanicek, S.J., Qian,
701 Y., Brown, S.D., Brandt, C.C., 2013. The genetic basis for bacterial mercury methylation.
702 *Science* 339, 1332-1335.

703 Pempkowiak, J., Cossa, D., Sikora, A., Sanjuan, J., 1998. Mercury in water and sediments of
704 the southern Baltic Sea. *The Science of The Total Environment* 213, 185-192.

705 Peretyazhko, T., Charlet, L., Grimaldi, M., 2006a. Production of gaseous mercury in
706 hydromorphic soils in the presence of ferrous iron: a laboratory study. *Eur. J. Soil Sci.* 57, 190-
707 199.

708 Peretyazhko, T., Charlet, L., Muresan, B., Kazimirov, V., Cossa, D., 2006b. Formation of
709 dissolved gaseous mercury in a tropical lake (Petit-Saut reservoir, French Guiana). *Science of*
710 *The Total Environment* 364, 260-271.

711 Porcella, D.B., 1994. Mercury in the environment: biogeochemistry, Mercury pollution
712 intergration and synthesis, pp. 3-19.

713 Poulton, S.W., Canfield, D.E., 2011. Ferruginous conditions: a dominant feature of the ocean
714 through Earth's history. *Elements* 7, 107-112.

715 Prah, F., Small, L., Eversmeyer, B., 1997. Biogeochemical characterization of suspended
716 particulate matter in the Columbia River estuary. *Marine Ecology Progress Series* 160, 173-
717 184.

718 Raimbault, P., Diaz, F., Pouvesle, W., Boudjellal, B., 1999. Simultaneous determination of
719 particulate organic carbon, nitrogen and phosphorus collected on filters, using a semi-automatic
720 wet-oxidation method. *Marine Ecology Progress Series* 180, 289-295.

721 Regnell, O., Ewald, G., Lord, E., 1997. Factors controlling temporal variation in methyl
722 mercury levels in sediment and water in a seasonally stratified lake. *Limnology and*
723 *oceanography* 42, 1784-1795.

724 Regnell, O., Tunlid, A., 1991. Laboratory study of chemical speciation of mercury in lake
725 sediment and water under aerobic and anaerobic conditions. *Applied and Environmental*
726 *Microbiology* 57, 789-795.

727 Regnell, O., Watras, C.J., 2018. Microbial mercury methylation in aquatic environments: a
728 critical review of published field and laboratory studies. *Environmental science & technology*
729 53, 4-19.

730 Riccardi, D., Guo, H.-B., Parks, J.M., Gu, B., Summers, A.O., Miller, S.M., Liang, L., Smith,
731 J.C., 2013. Why mercury prefers soft ligands. *The Journal of Physical Chemistry Letters* 4,
732 2317-2322.

733 Rigaud, S., Radakovitch, O., Couture, R.-M., Deflandre, B., Cossa, D., Garnier, C., Garnier, J.-
734 M., 2013. Mobility and fluxes of trace elements and nutrients at the sediment–water interface
735 of a lagoon under contrasting water column oxygenation conditions. *Applied Geochemistry* 31,
736 35-51.

737 Rolfhus, K.R., Fitzgerald, W.F., 2004. Mechanisms and temporal variability of dissolved
738 gaseous mercury production in coastal seawater. *Marine Chemistry* 90, 125-136.

739 Rosati, G., Heimbürger, L.-E., Melaku Canu, D., Lagane, C., Laffont, L., Rijkenberg, M.J.,
740 Gerringa, L.J., Solidoro, C., Gencarelli, C.N., Hedgecock, I.M., 2018. Mercury in the Black
741 Sea: New insights from measurements and numerical modeling. *Global Biogeochemical Cycles*
742 32, 529-550.

743 Saiz-Lopez, A., Sitkiewicz, S.P., Roca-Sanjuán, D., Oliva-Enrich, J.M., Dávalos, J.Z., Notario,
744 R., Jiskra, M., Xu, Y., Wang, F., Thackray, C.P., 2018. Photoreduction of gaseous oxidized
745 mercury changes global atmospheric mercury speciation, transport and deposition. *Nature*
746 *communications* 9, 1-9.

747 Schaefer, J.K., Morel, F.M.M., 2009. High methylation rates of mercury bound to cysteine by
748 *Geobacter sulfurreducens*. *Nature Geosci* 2, 123-126.

749 Skyllberg, U., 2008. Competition among thiols and inorganic sulfides and polysulfides for Hg
750 and MeHg in wetland soils and sediments under suboxic conditions: Illumination of

751 controversies and implications for MeHg net production. *Journal of Geophysical Research:*
752 *Biogeosciences* (2005-2012) 113.

753 Skyllberg, U., Qian, J., Frech, W., Xia, K., Bleam, W.F., 2003. Distribution of mercury, methyl
754 mercury and organic sulphur species in soil, soil solution and stream of a boreal forest
755 catchment. *Biogeochemistry* 64, 53–76.

756 Slowey, A.J., Brown, J.G.E., 2007. Transformations of mercury, iron, and sulfur during the
757 reductive dissolution of iron oxyhydroxide by sulfide. *Geochim. Cosmochim. Acta* 71, 877-
758 894.

759 Smith, R.M., Martell, A.E., 1976. *Critical stability constants: inorganic complexes*. Springer.

760 Soerensen, A.L., Schartup, A., Skrobonja, A., Bouchet, S., Amouroux, D., Liem-Nguyen, V.,
761 Björn, E., 2018. Deciphering the role of water column redoxclines on methylmercury cycling
762 using speciation modeling and observations from the Baltic Sea. *Global Biogeochemical Cycles*
763 32, 1498-1513.

764 Thouret, J.-C., Boivin, P., Labazuy, P., Leclerc, A., 2016. Geology, geomorphology and slope
765 instability of the maar lake Pavin (Auvergne, French Massif Central), Lake Pavin. Springer, pp.
766 155-174.

767 Tipping, E., 1994. WHAMC—A chemical equilibrium model and computer code for waters,
768 sediments, and soils incorporating a discrete site/electrostatic model of ion-binding by humic
769 substances. *Computers & Geosciences* 20, 973-1023.

770 Tisserand, D., Guéron, S., Razimbaud, S., Findling, N., Charlet, L., 2021. Acid volatile
771 sulfides and simultaneously extracted metals: A new miniaturized ‘purge and trap’ system for
772 laboratory and field measurements. *Talanta*, 122490.

773 Ullrich, S.M., Tanton, T.W., Abdrashitova, S.A., 2001. Mercury in the aquatic environment: A
774 review of factors affecting methylation. *Crit. rev. Environ. Sci. Technol.* 31, 241-293.

775 USEPA, 1998. Method 1630: Methyl Mercury in Water by Distillation, Aqueous
776 Ethylation, Purge and Trap, and Cold Vapor Atomic Fluorescence Spectrometry, in: USEPA
777 (Ed.), U.S. Environmental Protection Agency USEPA, Washington.

778 USEPA, 2002. Method 1631, Revision E: Mercury in Water by Oxidation, Purge and Trap, and
779 Cold Vapor Atomic Fluorescence Spectrometry, in: USEPA (Ed.), Washington.

780 Viollier, E., Inglett, P.W., Hunter, K., Roychoudhury, A.N., Van Cappellen, P., 2000. The
781 ferrozine method revisited: Fe (II)/Fe (III) determination in natural waters. *Applied*
782 *Geochemistry* 15, 785-790.

783 Viollier, E., Michard, G., Jézéquel, D., Pèpe, M., Sarazin, G., 1997. Geochemical study of a
784 crater lake: Lake Pavin, Puy de Dôme, France. Constraints afforded by the particulate matter
785 distribution in the element cycling within the lake. *Chemical Geology* 142, 225-241.

786 Wang, Y., Liu, J., Liem-Nguyen, V., Tian, S., Zhang, S., Wang, D., Jiang, T., 2022. Binding
787 strength of mercury (II) to different dissolved organic matter: The roles of DOM properties and
788 sources. *Science of The Total Environment* 807, 150979.

789 Watras, C., Bloom, N., 1994. The vertical distribution of mercury species in Wisconsin Lakes:
790 accumulation in plankton layers., in: Watras, C., Huckabee, J. (Eds.), *Mercury pollution:
791 integration and synthesis*. Lewis pub., pp. 137-185.

792 Xia, K., Skyllberg, U., Bleam, W., Bloom, P., Nater, E., Helmke, P., 1999. X-ray absorption
793 spectroscopic evidence for the complexation of Hg (II) by reduced sulfur in soil humic
794 substances. *Environmental science & technology* 33, 257-261.

795 Yang, S., Johnson, W.P., Black, F.J., Rowland, R., Rumsey, C., Piskadlo, A., 2020. Response
796 of density stratification, aquatic chemistry, and methylmercury to engineered and hydrologic
797 forcings in an endorheic lake (Great Salt Lake, USA). *Limnology and Oceanography* 65, 915-
798 926.

799 Zaferani, S., Pérez-Rodríguez, M., Biester, H., 2018. Diatom ooze—A large marine mercury
800 sink. *Science* 361, 797-800.

801 Zheng, W., Liang, L., Gu, B., 2011. Mercury Reduction and Oxidation by Reduced Natural
802 Organic Matter in Anoxic Environments. *Environmental Science & Technology* 46, 292-299.

803